Ground Moving Target Tracking with Context Information and a Refined Sensor Model

Michael Mertens
Department SDF
FGAN - FKIE
Wachtberg, Germany
Email: mertens@fgan.de

Martin Ulmke
Department SDF
FGAN - FKIE
Wachtberg, Germany
Email: ulmke@fgan.de

***Abstract*— For the detection of targets moving on ground, airborne *Ground Moving Target Indicator* (GMTI) radar is well-suited. In the tracking process, complex target dynamics, particularly stop and go maneuvers, and target masking due to Doppler blindness, often lead to track losses. By means of a refined sensor model it is possible to detect and handle such diverse target states. In addition, the generation of precise and continuous tracks from GMTI radar plots often is a demanding task due to terrain and technical obscuration and clutter. The exploitation of topographic background information such as road maps and terrain data is therefore highly desirable for the enhancement of track quality and track continuity.**
In the present paper these two aspects have been merged. The significant gain in track quality and track continuity is demonstrated in a number of simulation scenarios involving Doppler blindness and terrain obscuration.

Keywords: Ground moving target indicator radar (GMTI), road maps, target tracking, clutter notch, sensor model

I. Introduction

The state of the art sensor technology for the surveillance of ground traffic is airborne GMTI radar with space-time adaptive processing (STAP) [1]. The purpose of target tracking in this context is to support the surveillance by providing precise and continuous tracks of single vehicles as well as aggregations such as convoys. In a realistic scenario ground target tracking with airborne sensors often suffers from low visibility, high clutter and high target density. In addition complex target dynamics, e.g. stop and go maneuvers, and masking in doppler blindness situations can quickly lead to track losses. Thus the exploitation of as much a priori information as possible is highly desirable to improve the track quality and track continuity [2]–[4].
The present paper addresses the following issues on ground target tracking:

- road-map assisted target tracking
- using visibility information
- realistic sensor modeling

It describes an integration and application of Bayesian methods for exploiting digital road-maps and realistic GMTI sensor modeling as described in [5] and [6]. A detailed qualitative and quantitative analysis is provided for specific, relevant scenarios.

II. Tracking Algorithm

A. Remarks on Bayesian tracking

In general, BAYESian tracking algorithms perform sequential updates of the probability density function (pdf), $p(\mathbf{x}_k|\mathcal{Z}^k)$, of a target state $\mathbf{x}_k$ at time t_k, conditioned on the incoming measurements up to that time $\mathcal{Z}^k$, [7], [8]. Here, $\mathcal{Z}^k$ denotes all measurements of each scan up to the $k-$th scan, i.e. $\mathcal{Z}^k = \{Z_1, Z_2, \ldots, Z_k\}$.
Each update of $p(\mathbf{x}_k|\mathcal{Z}^k)$ consists of a prediction step that exploits the target dynamics model and road map information if it is available. The prediction is followed by a subsequent filter update step, where the newly received sensor data are processed by making use of the underlying sensor model. This process is illustrated by the following scheme:

$$\text{prediction:} \quad p(\mathbf{x}_{k-1}|\mathcal{Z}^{k-1}) \xrightarrow[\text{road maps}]{\text{dynamics}} p(\mathbf{x}_k|\mathcal{Z}^{k-1}) \tag{1}$$

$$\text{filter update:} \quad p(\mathbf{x}_k|\mathcal{Z}^{k-1}) \xrightarrow[\text{new data } Z_k]{\text{sensor model}} p(\mathbf{x}_k|\mathcal{Z}^k) \tag{2}$$

In the case of dense target situations, missing detections, and false alarms or clutter, the filtering step becomes intricate due to ambiguities in the data–targets assignment. Here, we apply a simple *probabilistic data association filter* (PDAF) [8] where a weighted average over all feasible plot–target assignments is performed. Since ground moving targets typically exhibit much less agility than, e.g. military air targets, the inclusion of accelerations into the state vector may not be necessary. Therefore, the target state at time t_k is defined by

$$\mathbf{x}_k = (\mathbf{r}_k^\top \;\; \dot{\mathbf{r}}_k^\top)^\top = (x_{k;1} \;\; \cdots \;\; x_{k;6})^\top \tag{3}$$

The Kalman filter assumes that the posterior density at every time step is Gaussian, i.e. completely described by its mean and covariance.

$$p(\mathbf{x}_{k-1}|\mathcal{Z}^{k-1}) = \mathcal{N}(\mathbf{x}_{k-1};\, \mathbf{x}_{k-1|k-1},\, \mathbf{P}^i_{k-1|k-1}) \tag{4}$$

with $\mathcal{N}$ denoting the normal distribution:

$$\mathcal{N}(\mathbf{x}; \mathbf{x}_0, \mathbf{P}) \equiv [\det(2\pi\mathbf{P})]^{-\frac{1}{2}} \exp[-\frac{1}{2}(\mathbf{x}-\mathbf{x}_0)^\top \mathbf{P}^{-1}(\mathbf{x}-\mathbf{x}_0)] \tag{5}$$

As widely accepted in the tracking literature [7], the Gaussian shape is preserved if the target dynamics is modelled by a

linear Markov process:

$$\mathbf{x}_k = \mathbf{F}_{k|k-1}\mathbf{x}_k + \mathbf{G}_{k|k-1}\mathbf{v}_k \tag{6}$$

which implies that the target state at time step t_{k+1} is determined by the state at the preceding time step t_k. In addition the measurement is assumed to be a linear function of the target state:

$$\mathbf{z}_k = \mathbf{H}_k\mathbf{x}_k + \mathbf{w}_k, \tag{7}$$

with Gaussian process and measurement noise, $\mathbf{v}_k$ and $\mathbf{w}_k$, respectively. When only the target position is measured, the measurement matrix $\mathbf{H}$ is reduced (in the simplest case) to

$$\mathbf{H} = \begin{pmatrix} \mathbf{1}_3 & \mathbf{0}_3 \end{pmatrix} \tag{8}$$

with three-dimensional unity and zero matrices $\mathbf{1}_3$ and $\mathbf{0}_3$. The filtering of the hypotheses is carried out within the well known Kalman formalism. The estimated target state in the k-th scan is described by a normal mixture of $n_k + 1$ individual track hypotheses, one for each feasible association of the current predicted track with each of the n_k sensor plots and one for the hypothesis that all detections are false alarms (*missed-detection* hypothesis, index $i = 0$):

$$p(\mathbf{x}_k|\mathcal{Z}^k) = \sum_{i=0}^{n_k} p^i(\mathbf{x}_k|\mathcal{Z}^k) = \sum_{i=0}^{n_k} w_k^i\, \mathcal{N}(\mathbf{x}_k;\, \mathbf{x}_{k|k}^i,\, \mathbf{P}_{k|k}^i). \tag{9}$$

The subscripts, $k|k$, at the mean $\mathbf{x}_{k|k}^i$ and covariance $\mathbf{P}_{k|k}^i$ in (9) reflect the dependence of estimates at time step k on all measurements up to the same time step, $\mathcal{Z}^k = \{Z_1, Z_2, \ldots, Z_k\}$. The (un-normalized) hypotheses weights w_k^i are given by the likelihood function:

$$w_k^i = \begin{cases} \frac{P_d}{f_c}\mathcal{N}(\mathbf{z}_{k+1}^j;\, \mathbf{H}_{k+1}\mathbf{x}_{k+1|k}^i,\, \mathbf{S}_{k+1}^{ij}), & \text{if } j > 0 \\ (1 - P_d), & \text{if } j = 0 \end{cases} \tag{10}$$

with the clutter density f_c and the probability of detection P_d entering as sensor parameters. In the PDAF treatment [8], the weighted sum (9) is approximated by a single normal distribution conserving first and second moments (*second order moment matching*) leading, typically, to reliable results for not too dense target and clutter situations. A more sophisticated *multi hypothesis tracker* (MHT) scheme for GMTI application has been described in [9].

B. Track extraction

For extracting a track of a road target, we apply the following simple approach: After projection onto the road each sensor plot serves as a seed for a new track with a certain covariance. The covariance determines the gate for possible associations of the track seed with sensor plots of the next scan. If a new plot cannot be assigned to a track seed, it generates a new track seed. If a track seed cannot be assigned to one of the sensor plots, it is discarded. If, however, such an assignment is possible the position of the track seed is shifted to the new plot position. After a series of n (typically $n = 3$) successful assignments, the track is established and then further processed according to the prediction and update scheme described above.

C. Refined sensor model

Starting point for a refined sensor model is the observation that the detection probability for the measurement process depends on the kinematic state of the target, i.e. $P_d = P_d(\mathbf{x}_k)$. An important reason for the absence of a measurement is *Doppler blindness*: it occurs when the target is in the clutter notch of the sensor, i. e. it has only a small difference in radial velocity relative to the surrounding main lobe clutter either because of the target-sensor geometry or because of a stopping maneuver. In these cases a discrimination from the main lobe clutter around the target is no longer possible.
Mathematically the clutter notch can be described in cartesian coordinates by projecting the target's speed on the direction vector between target and sensor:

$$n_c(\mathbf{x}_k) = \dot{\vec{\mathbf{r}}}_{target} \cdot \frac{\vec{\mathbf{r}}_{target} - \vec{\mathbf{r}}_{sensor}}{|\vec{\mathbf{r}}_{target} - \vec{\mathbf{r}}_{sensor}|} \quad . \tag{11}$$

Doppler blindness inevitably leads to a strong decrease of the detection probability. In this case the location of such a notch is determined by the target's kinematic state and the target-sensor geometry. On the other hand its width can be described by the sensor parameter MDV, the ***m**inimum **d**etectable **v**elocity*.
The state-dependent detection probability is introduced into the algorithm by assuming that for $|n_c(\mathbf{x}_k)| <$ MDV it holds that $P_d < \frac{1}{2}P_d^0$:

$$P_d(\mathbf{x}_k) = P_d^0 \cdot \left[1 - \exp\left\{-\log 2 \left(\frac{n_c(\mathbf{x}_k)}{\text{MDV}}\right)^2\right\}\right]. \tag{12}$$

with P_d^0 being the saturated detection probability far off the clutter notch region. The function $n_c(\mathbf{x}_k)$ is now linearized around the predicted state estimate $\mathbf{x}_{k|k-1}$:

$$n_c(\mathbf{x}_k) \approx z_k - \mathbf{H}_k\,\mathbf{x}_k \ , \tag{13}$$

with the quantities z_k and $\mathbf{H}_k$ given by

$$z_k = n_c(\mathbf{x}_{k|k-1}) + \mathbf{H}_k\,\mathbf{x}_{k|k-1} \tag{14}$$

$$\mathbf{H}_k = -\left.\frac{\partial n_c(\mathbf{x}_k)}{\partial \mathbf{x}_k}\right|_{\mathbf{x}_k = \mathbf{x}_{k|k-1}} . \tag{15}$$

Now the second factor in equation (12) can be rewritten as a normal distribution, yielding

$$P_d(\mathbf{x}_k) = P_d^0 \cdot \left[1 - \frac{\text{MDV}}{\sqrt{\log 2/\pi}}\,\mathcal{N}\left(z_k; \mathbf{H}_k\,\mathbf{x}_k, \frac{\text{MDV}^2}{2\log 2}\right)\right] . \tag{16}$$

Inserting the linearized $P_d(\mathbf{x}_k)$, consisting of two addends, into the likelihood function (10), we obtain for each detection a sum of two components and, thus, in total $2(n_k + 1)$ components in the filtered pdf (9) (see [5], [6] for details). In that way, the additional component coming from $P_d(\mathbf{x}_k)$ serves as a ficticious measurement which in case of a plot–track association removes probability density out of the clutter notch

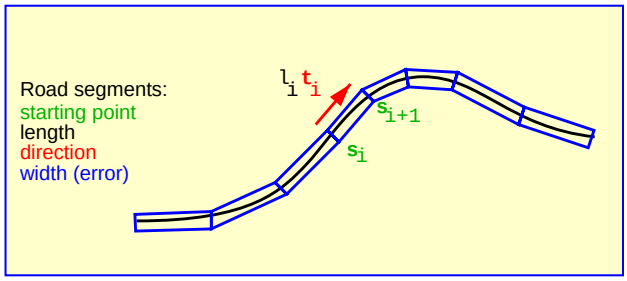

Fig. 1. Representation of a road.

hypothesis, while for a missed detection it shifts probability density into the clutter notch hypothesis.

D. Road Constraints

A given road is mathematically described by a continuous 3D curve $\mathcal{R}^*$ in Cartesian ground coordinates. Let $\mathcal{R}^*$ be parameterized by the corresponding arc length l: $\mathcal{R}^* : l \mapsto \mathcal{R}^*(l)$. In a digitized road map $\mathcal{R}^*$ is approximated by a polygonal curve $\mathcal{R}$ defined by piecewise linear segments. The curve $\mathcal{R}$ may be characterized by n_r node vectors

$$\mathbf{s}_m = \mathcal{R}^*(l_m), \quad m = 1, \ldots, n_r. \tag{17}$$

From these quantities $n_r - 1$ normalized tangential vectors

$$\mathbf{t}_m = \frac{\mathbf{s}_{m+1} - \mathbf{s}_m}{|\mathbf{s}_{m+1} - \mathbf{s}_m|}, \quad m = 1, \ldots, n_r - 1 \tag{18}$$

can be derived. The Euclidian distance $|\mathbf{s}_{m+1} - \mathbf{s}_m|$ between two adjacent node vectors, however, is usually not identical to the distance $\lambda_m = l_{m+1} - l_m$ actually covered by a vehicle when it moves from $\mathbf{s}_m$ to $\mathbf{s}_{m+1}$ along the road. Besides the vectors $\mathbf{s}_m$, the scalar quantities $\lambda_m \geq |\mathbf{s}_{m+1} - \mathbf{s}_m|$ should therefore enter into the road model to make it more realistic. The differences $\lambda_m - |\mathbf{s}_{m+1} - \mathbf{s}_m|$ can evidently serve as a quantitative measure of the discretization errors. Using the indicator function defined by

$$\chi_m(l) = \begin{cases} 1 & \text{for } l \in [l_m, l_{m+1}) \\ 0 & \text{otherwise} \end{cases}, \tag{19}$$

with $m = 1, \ldots, n_r - 1$, we obtain a mathematically simple description of the polygon curve $\mathcal{R}$, by which the road $\mathcal{R}^*$ is approximated:

$$\mathcal{R} : l \in [l_1, l_{n_r}) \mapsto \mathcal{R}(l) = \sum_{m=1}^{n_r - 1} \left[\mathbf{s}_m + (l - l_m)\mathbf{t}_m\right] \chi_m(l)$$
$$\text{with:} \quad \mathcal{R}^*(l_m) = \mathcal{R}(l_m) = \mathbf{s}_m, \quad m = 1, \ldots, n_r. \tag{20}$$

The accuracy by which the road is represented by the node vectors $\mathbf{s}_m$ can be described by a covariance matrix $\mathbf{R}_m$ characteristic of each node m. See Fig. 1 for illustration. In case of targets moving on road it seems reasonable to describe the kinematical state vector $\mathbf{x}_k^r$ of road targets at time t_k by its position on the road l_k (i.e. the arc length of the curve) and its scalar speed $\dot{l}_k$: $\mathbf{x}_k^r = (l_k, \dot{l}_k)^\top$. The model for describing the dynamical behavior of road targets is therefore a 2D version of (6). By making use of the related transition density $p(\mathbf{x}_k^r|\mathbf{x}_{k-1}^r)$ the predicted density in road coordinates is given by

$$p(\mathbf{x}_k^r|\mathcal{Z}^{k-1}) = \int p(\mathbf{x}_k^r|\mathbf{x}_{k-1}^r)\, p(\mathbf{x}_{k-1}^r|\mathcal{Z}^{k-1})\, d\mathbf{x}_{k-1}^r. \tag{21}$$

Now we face the problem, that the target dynamics is given in road coordinates while the measurements and, hence, the filter update is performed in cartesian ground coordinates. In principle, the Bayesian formalism discussed in Section II-A can be applied to road targets, if there exists a transformation operator $\mathcal{T}_{g \leftarrow r}$ which transforms the predicted density $p(\mathbf{x}_k^r|\mathcal{Z}^{k-1})$ from road to ground coordinates:

$$\underbrace{p(\mathbf{x}_k^r|\mathcal{Z}^{k-1})}_{\text{in road coordinates}} \xrightarrow[\text{road map errors}]{\text{road network}} \underbrace{p(\mathbf{x}_k^g|\mathcal{Z}^{k-1})}_{\text{in ground coordinates}} \tag{22}$$

In general such a transformation is highly nonlinear, and the structure of probability densities in terms of Gaussian sums cannot be preserved. Linearity is, however, conserved if one employs linearized road segments for the mapping between road and ground coordinates, as in (20). When available in ground coordinates, the linearized versions of the transforms from ground coordinates to sensor coordinates and vice versa, $\mathbf{t}_{s \leftarrow g}$ and $\mathbf{t}_{g \leftarrow s}$, can be used to represent the densities in sensor coordinates, where the filtering step is to be performed. In this case, the density in ground coordinates, $p(\mathbf{x}_k^g|\mathcal{Z}^{k-1})$, can be written as a sum over the road segments considered:

$$p(\mathbf{x}_k^g|\mathcal{Z}^{k-1}) = \sum_{m=1}^{n_r - 1} p(\mathbf{x}_k^g|m, \mathcal{Z}^{k-1})\, p(m|\mathcal{Z}^{k-1}). \tag{23}$$

In (23), $p(m|\mathcal{Z}^{k-1})$ denotes the probability that the target moves on segment m given the accumulated sensor data $\mathcal{Z}^{k-1}$. Its explicit form is given in references [5], [6]. The densities $p(\mathbf{x}_k^g|m, \mathcal{Z}^{k-1})$ can be calculated from the probability density in road coordinates and are approximately given by Gaussians. In the case of multiple roads with junctions, the sum of weights $p(m|\mathcal{Z}^{k-1})$ over the segments of a given road is proportional to the "road probability", i. e. the probability that the target is somewhere on that given road. The filtering step (see 10) recalculates the weight of each road segment and can, hence, also reweight the total road probabilities. The inverse transform from cartesian to road coordinates is simply provided by individually projecting the densities $p(\mathbf{x}_k^g|m, \mathcal{Z}^k)$ on the road (i.e. after the filtering step). Before the subsequent prediction is performed, it seems reasonable (and in the PDAF spirit) to apply a second-order approximation to the mixture densities:

$$p(\mathbf{x}_k^r|\mathcal{Z}^k) = \sum_{m=0}^{n_r} p(m|\mathcal{Z}^k) p(\mathbf{x}_k^r|m, \mathcal{Z}^k) \approx \mathcal{N}\big(\mathbf{x}_k^r;\, \mathbf{x}_{k|k}^r,\, \mathbf{P}_{k|k}^r\big). \tag{24}$$

A sketch of the road-map assisted tracking filter described above is given in Figure 2.

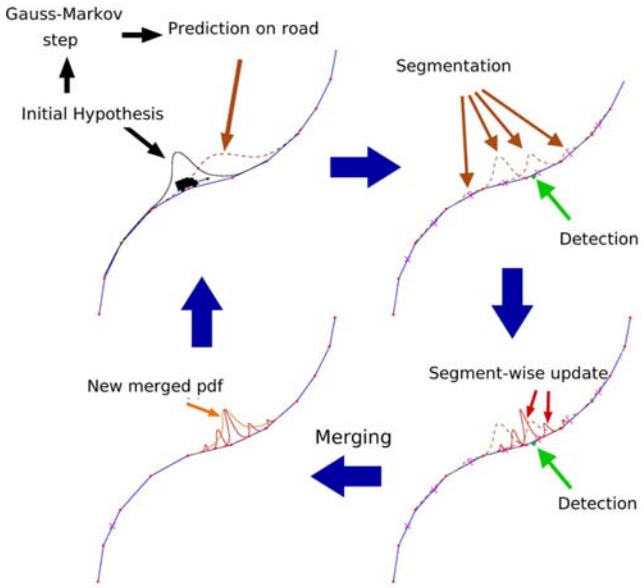

Fig. 2. Scheme of the road-map assisted tracking filter.

E. Terrain obscuration

Besides technical obscuration by the clutter notch of the sensor, the target may become invisible by the terrain, vegetation or tunnels. Such visibility information can, in principle, be derived from vector maps in combination with the sensor–target geometry. For road targets, the visibility may well be described by a road segment dependent detection probability $P_d(\mathbf{x})$ via P_d^0. That means the detection probability (12) obtains an additional dependence on the corresponding road segment m. In the case of a mountain in the line of sight, $P_d(\mathbf{x})$ may vary in time due to the sensor movement, while in the case of a tunnel $P_d(\mathbf{x}) = 0 = \text{const}$. If included into the tracking filter, missing detections will amplify the weights on segments with low $P_d(\mathbf{x})$ (see (10)). As in the case of the clutter notch, such negative sensor evidence can, therefore, contribute to the determination of the target state. A detection that fits to the actual target track, on the other hand, will decrease the weight on low-P_d segments.

III. Scenarios and Results

In order to illustrate the performance of the tracking filter qualitatively, we consider two rather difficult tracking situations of a branching road with and without terrain obscuration and the situation of a target performing a stop and go maneuver. Finally we will show a quantitative comparison of tracking filters with and without the exploitation of road-map and clutter notch information. All results are based on simulation scenarios.

A. Road with a junction

The target moves with constant speed of $40m/s$ along the road and passes a junction under an acute angle - the most difficult situation since the scattering of the measurements inhibits the separation of roads close to the junction. Fig. 3 depicts the scenario with roads (blue), true target positions (red), measurement plots (yellow crosses) and estimated tracks (white). From left to right we show the results for the PDAF tracker a) including road-map and clutter notch information, b) only with clutter notch information, and c) without exploiting additional information. In case a) only the track on the road with the largest weight is plotted. Measurement errors in azimuth, range, and height (the latter may be given by a projection onto a digital height model) are: $\Delta\phi = 0.25°, \Delta\text{r} = 20m$ and $\Delta\text{h} = 20m$. Apparently, here all trackers are able to follow the true track more or less faithfully, but the road-map information significantly improves the track precision (see error ellipses at the top of the track). Tracker b) and c) provide almost identical results, for there is no clutter notch problematic in this scenario.
For larger measurement errors ($\Delta\phi = 0.75°, \Delta\text{r} = 40m$ and $\Delta\text{h} = 40m$) the discrimination between the two roads is possible only after a number of scans when the distance between the roads becomes larger than the measurement errors. Closely after the intersection the two road probabilities are fluctuating around 0.5. The jumps in the track occur because only the road track with the highest probability is plotted.

B. Road with a junction with terrain obscuration

The tracking becomes more difficult if the intersection region is not visible to the sensor (Fig. 4). In the absence of measurements, the pure PDAF tracker just extrapolates the last filtered target state, the covariances grow and the track can be picked up by almost any false alarm. In practice this situation would lead to a track loss. The result is similar when clutter notch information is taken into account. If, however, knowledge of the terrain obscuration is not provided, the tracking behavior is different (Fig. 5): Here the missing detections shift probability density into the clutter notch hypothesis. The target is only “allowed” to move in cross–range direction to the sensor (which is located in the north-west direction), but the range rate need to be significantly below the MDV. In this case the correct target position after the obscuration is not picked up. The track is lost. Using road-map information, there is of course no knowledge on which road the target is, but the ignorance is confined to the undetectable region, and after a new detection the track is immediately picked up at the correct position.

C. Doppler blindness

An easy maneuver for a ground target to prevent from being detected by a GMTI radar is to make a stop. Such a situation is depicted in Fig. 6. Here the target moves with a maximum speed of $20m/s$ along the road. While the pure PDAF tracker quickly looses the track (r.h.s.), the knowledge on the clutter notch confines the track in cross–range direction as there is an additional hypothesis available for the interpretation of the sensor output, namely a target with range rate below MDV. Additional road-map information further constrains the track in road direction and therefore after a few successive missed

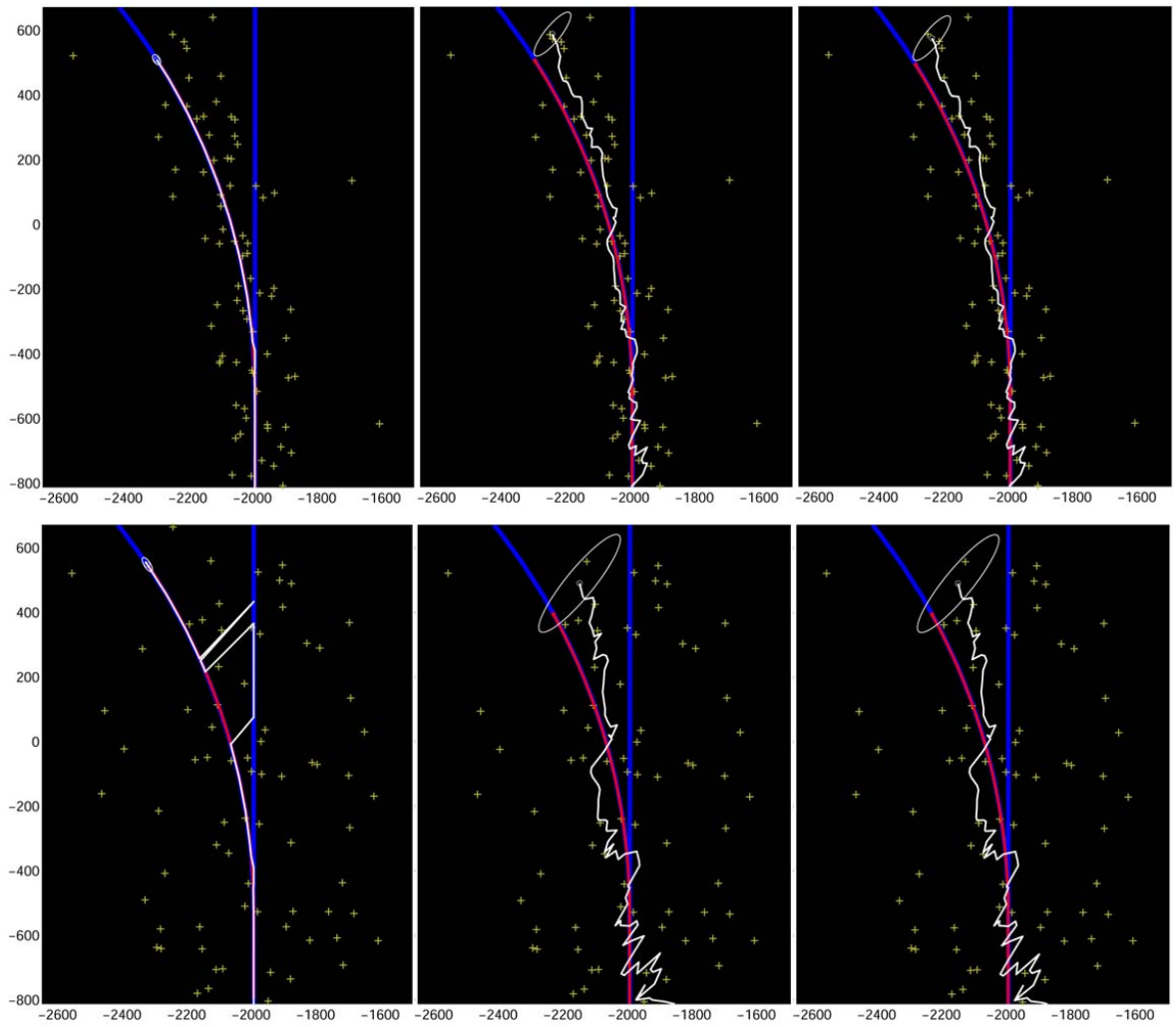

Fig. 3. Scenario and track results for PDAF trackers a) with road-map and clutter notch information, b) with only clutter notch information, c) without additional information (from left to right). Top: $\Delta\phi = 0.25°, \Delta\mathrm{r} = 20m$ and $\Delta\mathrm{h} = 20m$. Bottom: $\Delta\phi = 0.75°, \Delta\mathrm{r} = 40m$ and $\Delta\mathrm{h} = 40m$. Units are meter on both axes.

detections a stopping target is quickly detected. The estimate remains close to the tracked stopping position until new measurements arrive which are then picked up immediately. In general the interplay between clutter notch and road map processing is optimal when the road goes in range direction.

D. Numerical results

In order to assess the performance of the presented algorithm, we perform a Monte Carlo test (50 runs), considering a scenario that contains a target stop over 50 scans and a long and a short terrain obscuration. Scenario and tracking results for a specific random seed are shown in Fig. 7. The following quantities are calculated and plotted in Fig. 8:

- estimated rms-position error: $\sigma_{\text{total}} = \sqrt{\sigma_x^2 + \sigma_y^2 + \sigma_z^2}$
- target location error (TLE): $|\mathbf{r}_{\text{estimate}} - \mathbf{r}_{\text{truth}}|$
- target speed error (TSE): $|\mathbf{v}_{\text{estimate}} - \mathbf{v}_{\text{truth}}|$

Incorporating the topographic context information and using the refined sensor model leads to an obvious improvement in the target position estimate. In situations with high P_d, the error typically is reduced by a factor of $2 \sim 3$. When the target becomes invisible due to a stop or terrain masking, the gain can even be much larger. The improvement in the velocity estimate is not so pronounced, except for the case of a stopping target which is quickly detected only if clutter notch and road-map information is taken into account.

IV. Conclusions

In this work we have presented an algorithm to track ground moving targets by airborne radar. It incorporates context information such as road-map and terrain data and in addition a refined sensor model to include the clutter notch of the sensor in the tracking process. Results based on simulation scenarios show a significant improvement of the tracking performance in terms of track precision and track continuity. The latter is particularly important in the case of dense target situations. Algorithmic extensions to multiple and dense target situations are in progress.

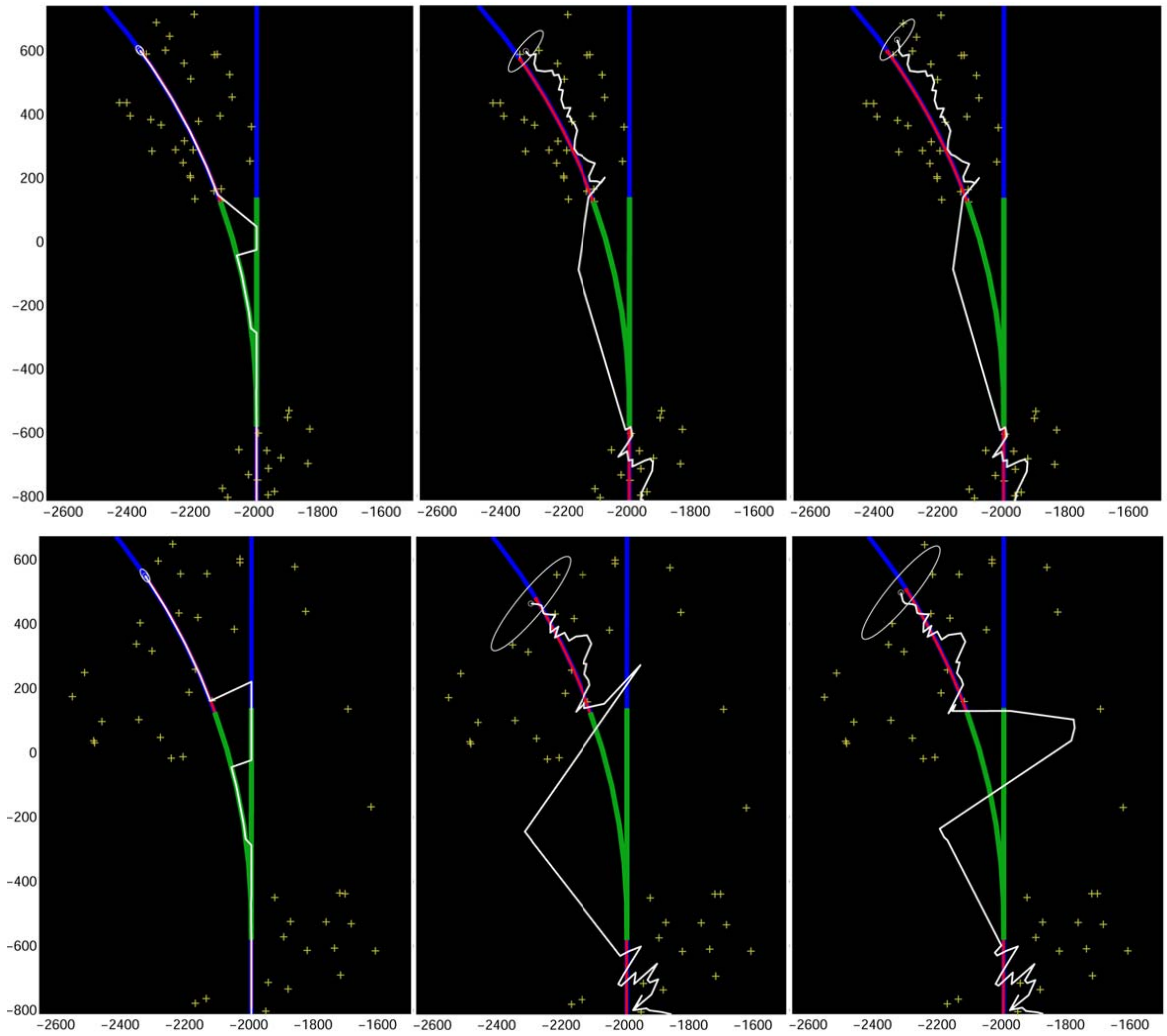

Fig. 4. Same scenario as in Fig. 3 but with an additional terrain obscuration (green) at the intersection. Top: $\Delta\phi = 0.25°, \Delta\mathrm{r} = 20m$ and $\Delta\mathrm{h} = 20m$. Bottom: $\Delta\phi = 0.75°, \Delta\mathrm{r} = 40m$ and $\Delta\mathrm{h} = 40m$. Units are meter on both axes.

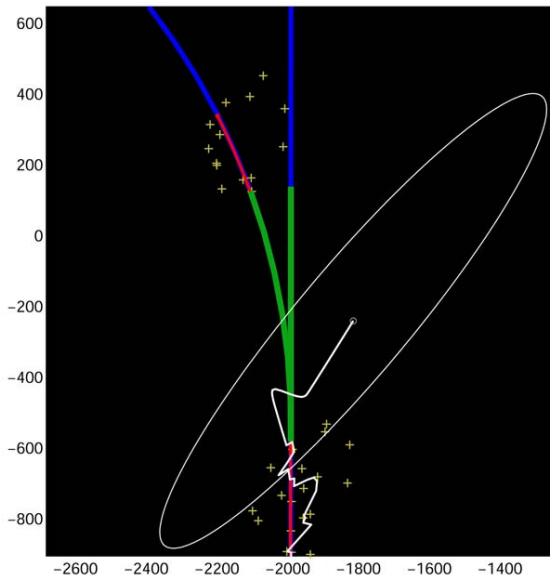

Fig. 5. Same scenario as in Fig. 4. Tracker uses clutter notch but no terrain information. $\Delta\phi = 0.25°, \Delta\mathrm{r} = 20m$ and $\Delta\mathrm{h} = 20m$.

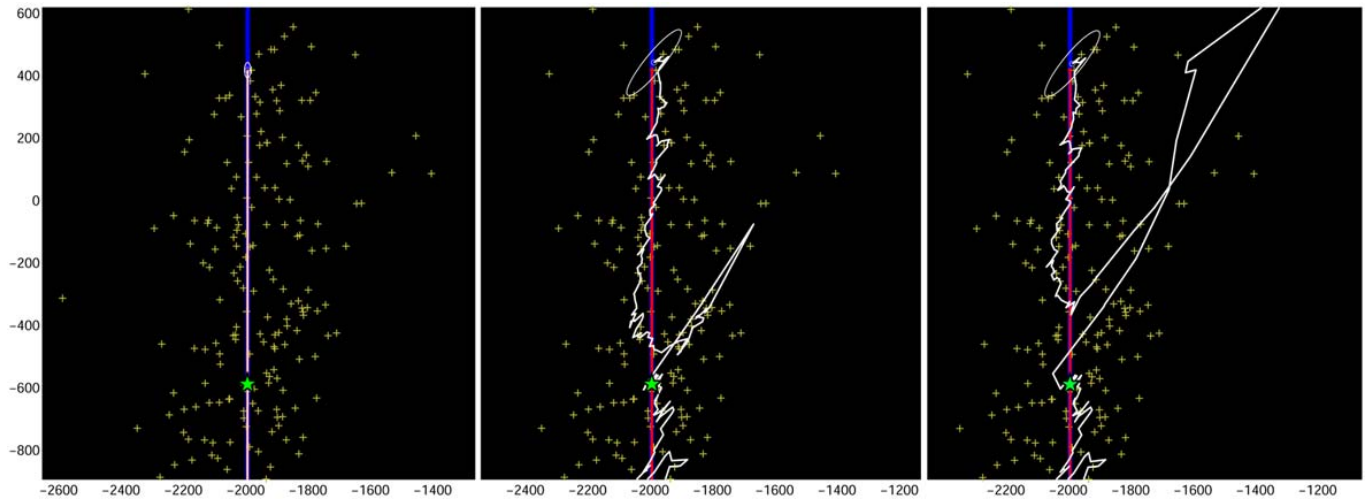

Fig. 6. Stop and go maneuver of a road target. Green star denotes the stop position. PDAF trackers a) with road-map and clutter notch information, b) with only clutter notch information, c) without additional information (from left to right). $\Delta\phi = 0.5°, \Delta\mathrm{r} = 30m, \Delta\mathrm{h} = 30m, \mathrm{MDV} = 3m/s$.

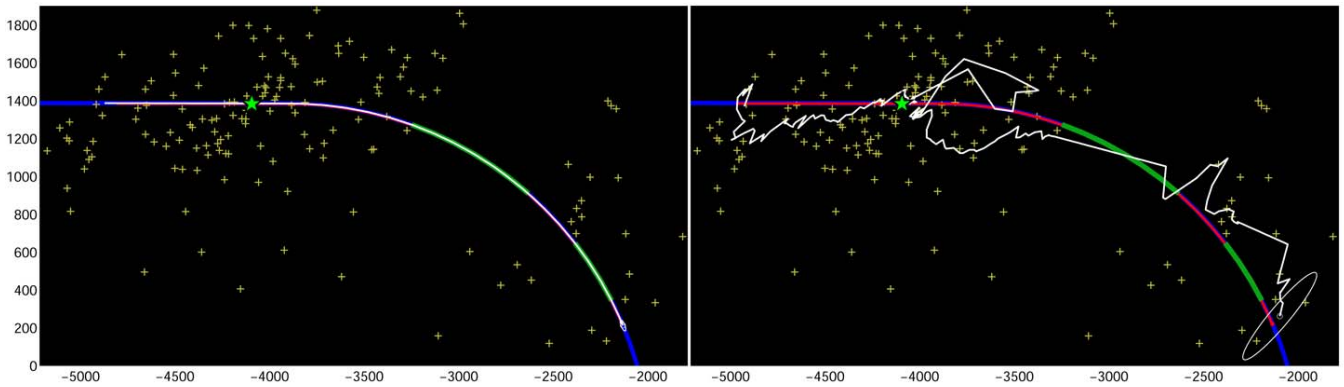

Fig. 7. Scenario and track results including a target stop (green star) and a long and a short terrain obscuration (green lines). Left: PDAF with clutter notch and road-map information; right: pure PDAF. $\Delta\phi = 1°, \Delta\mathrm{r} = 50m, \Delta\mathrm{h} = 50m, \mathrm{MDV} = 2m/s$.

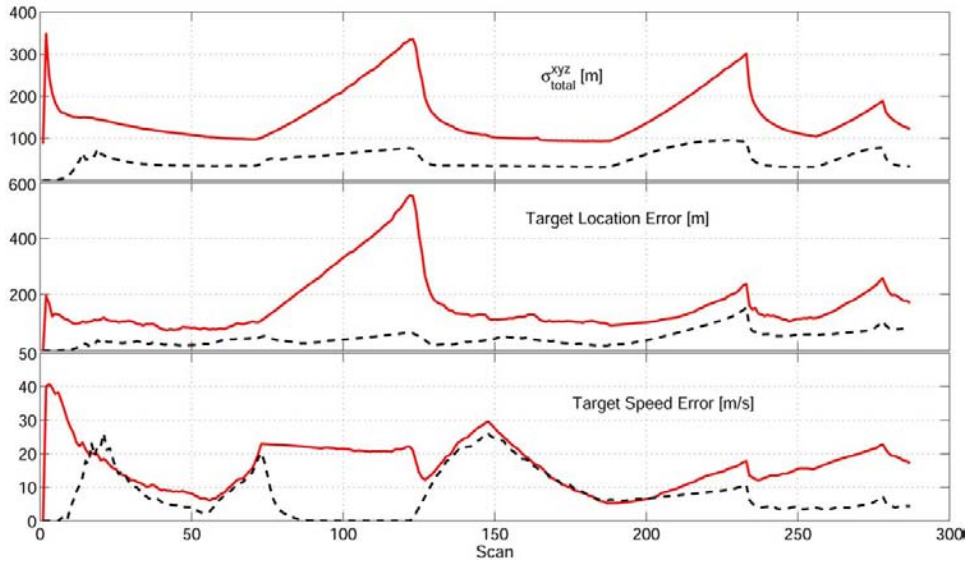

Fig. 8. MC results for the scenario in Fig. 7, averaged over 50 runs. Solid line: pure PDAF; dashed line: PDAF including clutter notch and road-map information. $\Delta\phi = 1°, \Delta\mathrm{r} = 50m, \Delta\mathrm{h} = 50m, \mathrm{MDV} = 2m/s$.

REFERENCES

[1] R. Klemm, *Space-time adaptive processing - principles and applications*. IEE Publishers, 1998.

[2] T. Kirubarajan, Y. Bar-Shalom, K. R. Pattipati, and I. Kadar, "Large scale ground target tracking with single and multiple MTI sensors," in *Multitarget-Multisensor Tracking Applications and Advances III* (Y. Bar-Shalom and W. D. Blair, eds.), Boston, MA: Artech House, 2000.

[3] P. J. Shea, T. Zadra, D. Klamer, E. Frangione, and R. Brouillard, "Improved state estimation through use of roads in ground tracking," in *Proc. of Signal and Data Processing of Small Targets* (O. E. Drummond, ed.), vol. 4048, pp. 321–332, SPIE, 2000.

[4] C. Agate and K. J. Sullivan, "Road-constraint target tracking and identification using a particle filter," in *Proc. of Signal and Data Processing of Small Targets* (O. E. Drummond, ed.), vol. 5204, SPIE, 2003.

[5] W. Koch, "Ground target tracking with STAP-Radar: Selected tracking aspects," in *Applications of Space-Time Adaptive Processing* (R. Klemm, ed.), London: Institution of Electrical Engineers, 2004.

[6] M. Ulmke and W. Koch, "Road-map assisted ground moving target tracking," *IEEE Transactions on Aerospace and Electronic Systems*, vol. 42, pp. 1264–1274, October 2006.

[7] S. Blackman and R. Popoli, *Design and Analysis of Modern Tracking Systems*. Artech House, Boston MA, 1999.

[8] Y. Bar-Shalom and X.-R. Li, *Estimation and Tracking: Principles, Techniques, and Software*. Boston MA: Artech House, 1993.

[9] J. Koller and M. Ulmke, "Multi hypothesis track extraction and maintenance of GMTI sensor data," in *Proceedings of the Eighth International Conference on Information Fusion*, (Philadelphia, USA), International Society of Information Fusion, June 2005.